LUND UNIVERSITY

Single-laser shot fluorescence lifetime imaging on the nanosecond timescale using a Dual Image and Modeling Evaluation algorithm

Ehn, Andreas; Johansson, Olof; Arvidsson, Andreas; Aldén, Marcus; Bood, Joakim

[Link to publication]

Single-laser shot fluorescence lifetime imaging on the nanosecond timescale using a Dual Image and Modeling Evaluation algorithm

Andreas Ehn,* Olof Johansson, Andreas Arvidsson, Marcus Aldén, and Joakim Bood

Division of Combustion Physics, Lund University, Box 118, SE-221 00 Lund, Sweden
*andreas.ehn@forbrf.lth.se

Abstract: A novel technique, designated dual imaging and modeling evaluation (DIME), for evaluating single-laser shot fluorescence lifetimes is presented. The technique is experimentally verified in a generic gas mixing experiment to provide a clear demonstration of the rapidness and sensitivity of the detector scheme. Single-laser shot fluorescence lifetimes of roughly 800 ps with a standard deviation of ~120 ps were determined. These results were compared to streak camera measurements. Furthermore, a general fluorescence lifetime determination algorithm is proposed. The evaluation algorithm has an analytic, linear relationship between the fluorescence lifetime and detector signal ratio. In combination with the DIME detector scheme, it is a faster, more accurate and more sensitive approach for rapid fluorescence lifetime imaging than previously proposed techniques. Monte Carlo simulations were conducted to analyze the sensitivity of the detector scheme as well as to compare the proposed evaluation algorithm to previously presented rapid lifetime determination algorithms.

OCIS codes: (110.0110) Imaging systems; (110.2970) Image detection systems; (110.4155) Multiframe image processing; (110.3010) Image reconstruction techniques; (170.0170) Medical optics and biotechnology; (170.3650) Lifetime-based sensing.

References and links

1. E. B. van Munster and T. W. Gadella, "Fluorescence lifetime imaging microscopy (FLIM)," Adv. Biochem. Eng. Biotechnol. **95**, 143–175 (2005).
2. J. Lakowicz, *Principles of Fluorescence Spectroscopy*, 3rd ed. (Springer, 2006).
3. A. D. Scully, R. B. Ostler, D. Phillips, P. O'Neill, K. M. S. Townsend, A. W. Parker, and A. J. MacRobert, "Application of fluorescence lifetime imaging microscopy to the investigation of intracellular PDT mechanisms," Bioimaging **5**(1), 9–18 (1997).
4. R. Pepperkok, A. Squire, S. Geley, and P. I. H. Bastiaens, "Simultaneous detection of multiple green fluorescent proteins in live cells by fluorescence lifetime imaging microscopy," Curr. Biol. **9**(5), 269–274 (1999).
5. P. J. Verveer, F. S. Wouters, A. R. Reynolds, and P. I. H. Bastiaens, "Quantitative imaging of lateral ErbB1 receptor signal propagation in the plasma membrane," Science **290**(5496), 1567–1570 (2000).
6. H. E. Grecco, P. Roda-Navarro, A. Girod, J. Hou, T. Frahm, D. C. Truxius, R. Pepperkok, A. Squire, and P. I. H. Bastiaens, "In situ analysis of tyrosine phosphorylation networks by FLIM on cell arrays," Nat. Methods **7**(6), 467–472 (2010).
7. C.-W. Chang, D. Sud, and M.-A. Mycek, "Fluorescence lifetime imaging microscopy," Methods Cell Biol. **81**, 495–524 (2007).
8. T. Robinson, P. Valluri, H. B. Manning, D. M. Owen, I. Munro, C. B. Talbot, C. Dunsby, J. F. Eccleston, G. S. Baldwin, M. A. A. Neil, A. J. de Mello, and P. M. W. French, "Three-dimensional molecular mapping in a microfluidic mixing device using fluorescence lifetime imaging," Opt. Lett. **33**(16), 1887–1889 (2008).
9. T. Ni and L. A. Melton, "Fuel equivalence ratio imaging for methane jets," Appl. Spectrosc. **47**(6), 773–781 (1993).
10. T. Ni and L. A. Melton, "Two-dimensional gas-phase temperature measurements using fluorescence lifetime imaging," Appl. Spectrosc. **50**(9), 1112–1116 (1996).
11. A. Ehn, O. Johansson, J. Bood, A. Arvidsson, B. Li, and M. Aldén, "Fluorescence lifetime imaging in a flame," Proc. Combust. Inst. **33**(1), 807–813 (2011).
12. W. Koban, J. D. Koch, R. K. Hanson, and C. Schulz, "Toluene LIF at elevated temperatures: implications for fuel–air ratio measurements," Appl. Phys. B **80**(2), 147–150 (2005).

13. C. J. de Grauw and H. C. Gerritsen, "Multiple time-gate module for fluorescence lifetime imaging," Appl. Spectrosc. **55**(6), 670–678 (2001).
14. D. V. O'Conner and D. Phillips, *Time-Correlated Single Photon Counting* (Academic, 1984).
15. K. Dowling, S. C. W. Hyde, J. C. Dainty, P. M. W. French, and J. D. Hares, "2-D fluorescence lifetime imaging using a time-gated image intensifier," Opt. Commun. **135**(1-3), 27–31 (1997).
16. X. F. Wang, T. Uchida, and S. Minami, "A fluorescence lifetime distribution measurement system based on phase-resolved detection using an image dissector tube," Appl. Spectrosc. **43**(5), 840–845 (1989).
17. P. C. Schneider and R. M. Clegg, "Rapid acquisition, analysis, and display of fluorescence lifetime-resolved images for real-time application," Rev. Sci. Instrum. **68**(11), 4107–4119 (1997).
18. R. J. Woods, S. Scypinski, and L. J. Cline Love "Transient digitizer for the determination of microsecond luminescence lifetimes," Anal. Chem. **56**(8), 1395–1400 (1984).
19. D. S. Elson, I. Munro, J. Requejo-Isidro, J. McGinty, C. Dunsby, N. Galletly, G. W. Stamp, M. A. A. Neil, M. J. Lever, P. A. Kellett, A. Dymoke-Bradshaw, J. Hares, and P. M. W. French, "Real-time time-domain fluorescence lifetime imaging including single-shot acquisition with a segmented optical image intesifier," New J. Phys. **6**, 180 (2004).
20. P. I. H. Bastiaens and A. Squire, "Fluorescence lifetime imaging microscopy: spatial resolution of biochemical processes in the cell," Trends Cell Biol. **9**(2), 48–52 (1999).
21. G. Bunt and F. S. Wouters, "Visualization of molecular activities inside living cells with fluorescent labels," Int. Rev. Cytol. **237**, 205–277 (2004).
22. A. Esposito, C. P. Dohm, M. Bähr, and F. S. Wouters, "Unsupervised fluorescence lifetime imaging microscopy for high content and high throughput screening," Mol. Cell. Proteomics **6**(8), 1446–1454 (2007).
23. S. Kirkpatrick, C. D. Gelatt, Jr., and M. P. Vecchi, "Optimization by simulated annealing," Science **220**(4598), 671–680 (1983).
24. T. B. Settersten and M. A. Linne, "Modeling pulsed excitation for gas-phase laser diagnostics," J. Opt. Soc. Am. B **19**(5), 954–964 (2002).
25. R. A. Alberty and R. J. Silbey, *Physical Chemistry*, 2nd ed. (Wiley, New York, 1997), Chap 19.7.
26. A. Elder, S. Schlachter, and C. F. Kaminski, "Theoretical investigation of the photon efficiency in frequency-domain fluorescence lifetime imaging microscopy," J. Opt. Soc. Am. A **25**(2), 452–462 (2008).
27. A. Draaijer, R. Sanders, and H. C. Gerritsen, "Fluorescence lifetime imaging, a new tool in confocal microscopy," in *Handbook of Biological Confocal Microscopy*, J. B. Pawley, ed. (Plenum, New York, 1995), pp. 491–505.
28. J. McGinty, J. Requejo-Isidro, I. Munro, C. B. Talbot, P. A. Kellett, J. D. Hares, C. Dunsby, M A A. Neil, and P. M. W. French, "Signal-to-noise characterization of time-gated intensifiers used for wide-field time-domain FLIM," J. Phys. D Appl. Phys. **42**(13), 135103 (2009).
29. A. V. Agronskaia, L. Tertoolen, and H. C. Gerritsen, "High frame rate fluorescence lifetime imaging," J. Phys. D Appl. Phys. **36**(14), 1655–1662 (2003).
30. S. P. Chan, Z. J. Fuller, J. N. Demas, and B. A. DeGraff, "Optimized gating scheme for rapid lifetime determinations of single-exponential luminescence lifetimes," Anal. Chem. **73**(18), 4486–4490 (2001).

1. Introduction

Fluorescence lifetime imaging (FLI) designates a collection of optical measurement techniques that have been used for more than two decades [1,2]. These techniques determine radiative and nonradiative energy transfer probabilities, which are dependent on parameters such as temperature, pressure, and number densities of quenching species. Information about these parameters is of great interest in several scientific fields, such as biomedicine [3–7] and physical chemistry [8–12].

In FLI measurements, the aim is to characterize the temporal decays of the fluorescence signals, which generally are exponential. Several FLI schemes have been invented and successfully applied for extraction of temporal information [13–15]. These techniques are commonly divided into two subgroups depending on whether the fluorescence lifetime is extracted through analysis in the frequency or in the time domain. Furthermore, the image buildup could be performed by direct imaging or scanning the measurement area. These approaches are called wide-field imaging and laser scanning imaging, respectively. Detectors used in wide-field imaging, such as CCD cameras with intensifiers, allow significantly shorter total acquisition times for the experiment than scanning techniques, which require at least one laser pulse excitation per image pixel. The merits of wide-field imaging have been utilized for analysis in the temporal [9,10] as well as the frequency domain [16,17]. The wide-field concept opens up for capturing dynamic events on short timescales. Fluorescence lifetimes in the nanosecond range have been measured by Schneider and Clegg using FLI in the

frequency domain [17]. However, performing rapid FLI in the frequency domain requires longer acquisition times than pulse excited FLI in the temporal domain. In the temporal domain, Ni and Melton [9] performed single-laser shot measurements with a shortest presented lifetime of 14 ns, which is roughly 2-3 times longer than what typically is of interest [2–8,11], and they had to use an FL-to-signal intensity calibration curve to evaluate the data. In a follow-up paper, Ni and Melton used the SRLD algorithm proposed by Ashworth and associates [18] to determine the fluorescence lifetime. However, this time measured lifetimes were longer than 30 ns [10]. Microscopic FLI investigations in the field of biomedicine have been performed in the time domain by Elson et al [19]. In this work fluorescence lifetimes of a few nanoseconds were measured in single acquisition with a repetition rate of 20 fps, corresponding to an acquisition time of 50 ms. It should be noted that the demand on temporal resolution in microscopy generally is several orders of magnitudes lower. Therefore, laser systems with high repetition rates are used which also keeps the laser-pulse energy low enough not to perturb the sample.

The approach presented here aims at performing single-shot FLI measurements in a fluorescence-lifetime span of interest for the bio- and physical-chemistry community, which may be below 1 ns. The FLI concept presented here operates in the time domain. It takes the actual gain functions of the ICCD cameras into account and utilizes the shapes of these profiles in order to provide better signal-to-noise ratios than what is obtained with previously developed FLI schemes. High signal-to-noise ratios are of great importance, particularly when single-laser shot measurements are considered. FLI data are acquired in single laser shot, making the fluorescence lifetime itself the limitation for the temporal and spatial resolution of the dynamic event of interest. In order to illustrate the rapidness, accuracy and sensitivity of the technique in an intuitive way, the experiments were conducted in gaseous flows under turbulent flow conditions, with rapid velocities and relatively low number densities typically associated with gas-phase measurements. Our results show that this novel detector scheme has the capability to be used for; quenching free concentrations measurements [11], achieve quantitative pH measurements [3], measure quencher molecule concentration [8] (e.g. oxygen [12]) as well as temperatures [10], in single shot. Furthermore, the presented approach could improve instrumentation for imaging of biochemical processes within cells [20,21] and for high content screening [22].

2. Description of the technique

A picosecond laser was used for excitation and the FLI detector scheme is demonstrated using two intensified CCD cameras. The data-evaluation routine involves detailed characterization of the experimental setup; taking temporal jitter and shape of the gain functions into account. Using the current data-evaluation routine, 2D single-laser shot lifetime images of decay times shorter than 1 ns are, for the first time, provided. We call this image evaluation concept DIME (Dual Imaging and Modeling Evaluation), and it allows effective fluorescence lifetime imaging of transient events in one excitation, or in case of hardware accumulation, in one (dual-) image readout. In addition, a new fluorescence lifetime determination algorithm is presented called RGF-LD (ramped gain profile lifetime determination). When performed in combination with DIME, it allows accurate and sensitive single-shot fluorescence lifetime determination of virtually any lifetime.

The experimental setup is shown in Fig. 1. The fourth harmonic (266 nm) of a pulsed (10 Hz) Nd:YAG laser (Ekspla PL 2143C) with 30 ps pulse duration was focused into a laser sheet aligned into the probe volume. The pulse energy was on the order of 5-10 mJ. Toluene-seeded gas was ejected through a 2.2 mm diameter jet tube inserted at the center of a porous plug, which provides a controlled co-flow of gas shielding the central jet. Calibrated mass flow controllers were used to provide well characterized oxygen/nitrogen gas mixtures to the jet and co-flow through separate gas-supply systems. Two intensified CCD cameras (PI-MAX II, model numbers 7483-0001 and 7489-0008), one of which has a fast gate option, were

positioned in a right-angle configuration with a 70/30 beam splitter directing the signal to the two cameras. A gated MCP-PMT (Hamamatsu R5916U-50) detected the laser pulses before they reached the probe volume. The time separation between the MCP-PMT signal and a gate monitor pulse from one of the cameras was logged using a 3 GHz digital oscilloscope (LeCroy Wavemaster 8300), allowing single-shot jitter correction in the data analysis, as well as discrimination of single-shot data with large time jitter. Lifetime images were compared along a horizontal pixel row through the gas jet with streak-camera measurements. Grid images were recorded prior to each measurement in order to overlap the two camera images. An in-house code based on simulated annealing [23] was used to find an image transform that overlapped the two camera images pixel-by-pixel.
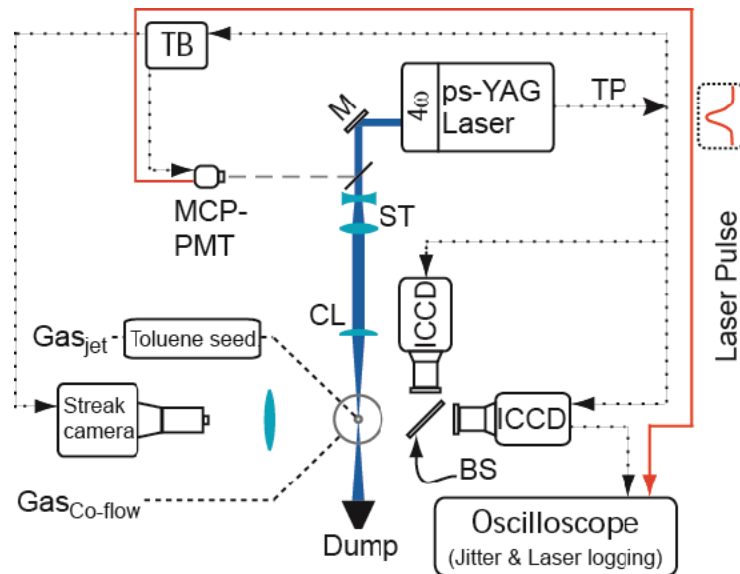

Fig. 1. Schematic illustration of the experimental setup. The laser beam is expanded using a spherical telescope (ST) and then focused to a laser sheet in the measurement volume with a cylindrical lens (CL). A trig pulse (TP) is sent to the two ICCD cameras and to a trigger box (TB) which triggers both the streak camera and the MCP-PMT. A 70/30 beam splitter (BS) is located in the front of the camera lenses.

From one single excitation, two PLIF images were recorded with different camera gain characteristics. Typical experimental results using 2 ns and 400 ns camera-gain widths are seen in Figs. 2a_exp and 2b_exp, respectively. The 2 ns camera has 512x512 pixels and the 400 ns camera has a resolution of 1024x1024 pixels. Both cameras were, however, hardware binned, providing an effective pixel resolution of 256x256. It should be stressed that for given gain widths, the gain profiles of these two cameras cannot be modified. Thus, after choosing widths of the gain functions, the profiles can merely be shifted in time. The shortest obtainable gain width was 2 ns for the current camera systems. Nevertheless, it will become clear later that it is not critical for the proposed technique to use a short gain width. The gain width of the other camera was chosen so that it would encompass the entire fluorescence decay signal. These gain functions were chosen in order to demonstrate the DIME concept and, at the same time, provide clear, pedagogic illustrations. It ought to be mentioned here that no distinction is made regarding whether the shapes of measured gain profiles stem from the gate voltage applied between the photocathode and the microchannel plate (MCP), the gain voltage over the MCP or both voltages.

Signals detected by the two cameras can be simulated if the laser pulse temporal profile, time jitter and camera-gain functions are known. The laser pulse was measured with the
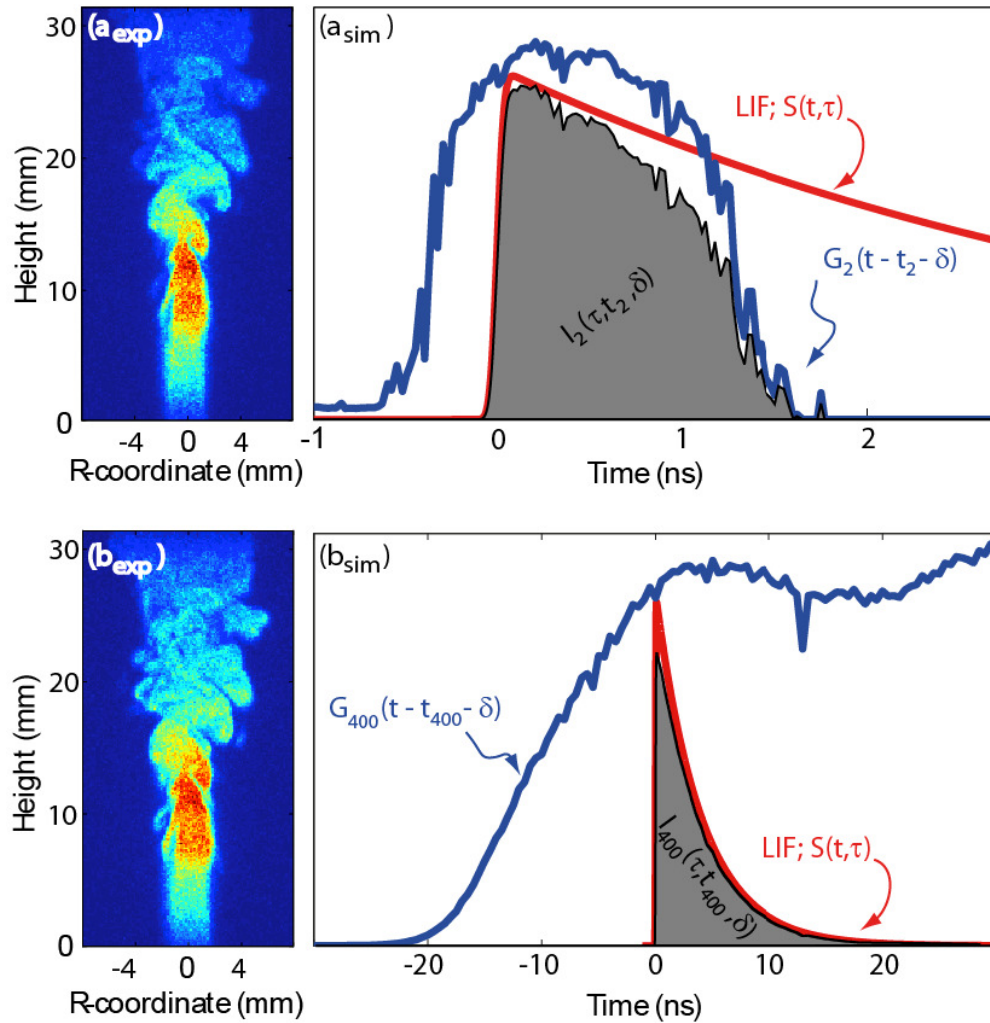
Fig. 2. PLIF images and graphical illustrations of signal simulations. Simultaneous, single-laser shot PLIF images of a toluene-seeded jet in a nitrogen co-flow are seen in (a_{exp}) and (b_{exp}) detected with a 2 ns and a 400 ns gated camera, respectively. In (a_{sim}) and (b_{sim}), graphical descriptions of simulations of ICCD-camera signal detection are displayed. The red curves are simulated LIF signals with lifetimes of 7 ns, the blue curve in (a_{sim}) is the 2 ns camera gain function while the rising flank of the 400 ns gain function is seen in (b_{sim}). The gray areas are the simulated signals detected by the two ICCD cameras, using Eq. (1).

streak camera and the temporal profile was found to be well described by a bell-shaped curve with 30 ps in full width half maximum (FWHM). The gain functions were measured by sequentially stepping the delay time between the camera gain and the laser pulse, while recording Rayleigh scattering from a flow of air. Recorded gain functions were corrected for differences in camera sensitivity at the Rayleigh and LIF wavelengths. To do this correction, sequential stepping of the gain profile delay time was performed while recording the Rayleigh and LIF signals. Ratios between these signals for each camera were formed and multiplied with the gain functions. To ensure that the experimental data were acquired with the same camera-gain functions that were used in the evaluation, the camera-gain curve mapping procedure was performed along with each experimental data set. The gain-curve functions seen in Figs. 2 a_{sim} and b_{sim} are measurement data that could be collected and implemented in the data analysis with higher signal-to-noise ratios. However, since the signal is based on

integration, the signal-to-noise ratio of the camera-gain curves is not crucial, allowing the gain-curve mapping measurements to be conducted fairly fast with few accumulations per time step.

Graphical descriptions of simulated signals are shown in Figs. 2a$_{sim}$ and Fig. 2b$_{sim}$. The red curves show the LIF signal, which is modeled as a single exponential decay convolved with the laser pulse, and it is denoted $S(t,\tau)$, where τ is the fluorescence lifetime. Test simulations of the LIF signal were performed for moderate excitation intensities with density matrix equations (DME) and rate equations (RE) following the guidelines presented by Settersten and Linne [24], neglecting spectral overlaps and detuning. The difference in evaluation of fluorescence lifetimes when using convolution, rate equations or density matrix equations approaches was less than 0.1%, justifying the choice of convolution, which is the least complicated of the three.

$G_2(t - t_2 - \delta)$ and $G_{400}(t - t_{400} - \delta)$ are the time-dependent camera gain functions of the two cameras, where details about the collection are incorporated. These functions are shown as blue curves in Figs. 2a$_{sim}$ and Fig. 2b$_{sim}$. The two variables, t_i and δ are the camera delay time and the time jitter, respectively. Note that the two gain curves are not top-hat shaped and that only the initial part of 400 ns gain profile is used unless the fluorescence lifetime is very long. It becomes clear from looking at the 400 ns gain profile that the gain width is only a number and does not consider the shape since the rise time is roughly 20 ns. The gray areas in Figs. 2a$_{sim}$ and Fig. 2b$_{sim}$ are the simulated signals in two corresponding pixels of the cameras, i.e. the integrated gray areas correspond to the signals recorded in these two corresponding pixels, short only of a constant. These integrated signals may be calculated using Eq. (1), with i being the camera index:

$$I_i\left(\tau,t_i,\delta\right) = \int_{-\infty}^{\infty} S\left(t,\tau\right)G_i\left(t - t_i - \delta\right)dt \tag{1}$$

A signal ratio is then defined:

$$D = \frac{I_2}{I_2 + I_{400}} \tag{2}$$

which is the signal fraction detected by the 2 ns gain width camera. With knowledge about the camera delay times (t_2 and t_{400}) and the time jitter (δ) for the set of LIF images analyzed, the ratio $D_s(\tau,t_2,t_{400},\delta)$ is simulated for a set of fluorescence lifetimes. If each D_s-value corresponds to a single value of τ, it is possible to express the fluorescence lifetime as a function of the signal ratio, $\tau(D_s)$, as shown in Fig. 3a. An experimental-ratio image, $D_e(x,y)$, is formed from the experimental LIF images (Fig. 2) using Eq. (2). By forming such a ratio between two experimental signals, inhomogeneities in the laser sheet as well as concentration variations are cancelled. Correspondingly, the initial intensity of the signal can be discarded in the simulations. To calculate a fluorescence-lifetime image from a single excitation, $\tau(D_s)$ is applied to each pixel value of $D_e(x,y)$. The FL image of the turbulent jet is shown in Fig. 3b. In the turbulent outer part downstream of the jet, the nitrogen co-flow mixes with the oxygen richer toluene seeded jet, resulting in longer fluorescence lifetimes, seen as brighter areas in Fig. 3b. For certain systems at fixed temperatures, the fluorescence lifetime is related to the oxygen concentration through the Stern-Volmer equation [25], providing a possibility for quantitative oxygen concentration determination without calibration.

For $D_s(\tau,t_2,t_{400},\delta)$ to be unambiguous with respect to τ, the derivative $dD_s/d\tau$ must not be zero, unless it is an inflection point. An analytic expression of $dD_s/d\tau$ offers a geometric interpretation of the unambiguity of $D_s(\tau)$. If the integrand, $S(t,\tau)G(t - t_i - \delta)$, is denoted $W_i(t,\tau)$, $D_s(\tau)$ can be written as
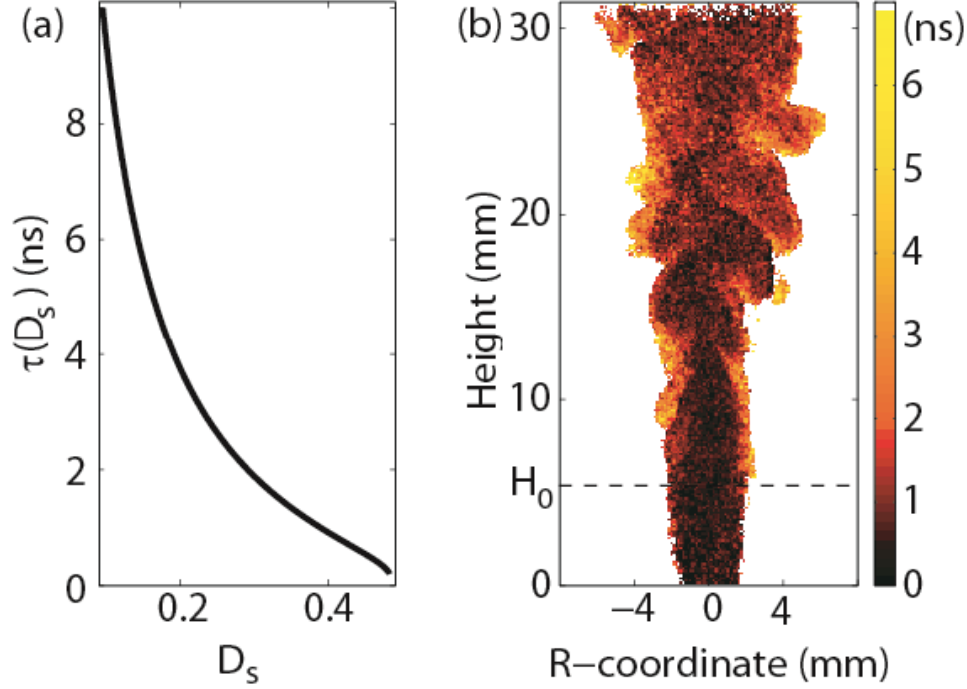
Fig. 3. Signal evaluation function and fluorescence lifetime image. (a) Fluorescence lifetime as a function of the simulated signal ratio, defined by Eq. (2). (b) Single-shot fluorescence lifetime image of a toluene seeded gas jet (N_2/O_2-mix) in a co-flow of nitrogen.

$$D_s = \frac{\int\limits_{-\infty}^{\infty} W_2(t,\tau)\,dt}{\int\limits_{-\infty}^{\infty}\left[W_2(t,\tau)+W_{400}(t,\tau)\right]dt} \tag{3}$$

Here, $W_i(t,\tau)$ could be interpreted as the (non-normalized) probability-density function of the time at which an electron reaches the phosphor in front of the CCD chip. In Figs. 2a$_{sim}$ and Fig. 2b$_{sim}$, $W_i(t,\tau)$ is seen as the solid black line at the boundary of the gray area. Taking the derivative of D_s with respect to τ while assuming the LIF signal to be described by a single exponential decay, the following expression is derived:

$$\frac{dD_s}{d\tau} = \frac{1}{\tau^2}\frac{\int\limits_{-\infty}^{\infty} W_2(t,\tau)\,dt \cdot \int\limits_{-\infty}^{\infty} W_{400}(t,\tau)\,dt}{\left\{\int\limits_{-\infty}^{\infty}\left[W_2(t,\tau)+W_{400}(t,\tau)\right]dt\right\}^2}\cdot\left[\underbrace{\frac{\int\limits_{-\infty}^{\infty} tW_2(t,\tau)\,dt}{\int\limits_{-\infty}^{\infty} W_2(t,\tau)\,dt}}_{E_2(t)}-\underbrace{\frac{\int\limits_{-\infty}^{\infty} tW_{400}(t,\tau)\,dt}{\int\limits_{-\infty}^{\infty} W_{400}(t,\tau)\,dt}}_{E_{400}(t)}\right] \tag{4}$$

$E_i(t)$ is the expectation value in time of $W_i(t,\tau)$, which is the time at which the gray area, in Fig. 2a$_{sim}$ and 2b$_{sim}$, are divided into equal halves. Thus for Eq. (3) to have a determinate solution, the expectation values of $W_2(t,\tau)$ and $W_{400}(t,\tau)$ must not coincide. It should be noted that single acquisitions with large time jitter, which increase the gain profile delay, could cause $dD_s/d\tau$ to be zero for the span of lifetimes investigated. Since the jitter was logged, such results were easily identified and rejected.

3. Evaluation of the DIME algorithm

The DIME FLI detector scheme was evaluated by comparing single-shot FL images with streak-camera (Optronis Optoscope S20) data of 900 accumulations since single-shot streak camera data were far too noisy for proper lifetime evaluation. The horizontal line where the streak-camera measurements were performed is marked with a dashed line located 5.4 mm downstream in the 2D lifetime image shown in Fig. 3b. At this height, referred to as H_0, the turbulence had not developed and thus it was possible to accumulate streak camera data. In Fig. 4, fluorescence lifetimes obtained with the FLI detector and the streak camera are displayed as circles and lines, respectively. In these measurements, the same buffer gas compositions were used for the co-flow and the toluene-seeded jet. Two measurements were conducted with different oxygen/nitrogen fractions; 10.5/89.5 and 17/83. Mean values (filled/open circles) and standard-deviations (error bars) were found for single pixels at H_0 from sets of ~150 single-shot FL images. Data with time jitter larger than one standard deviation of the time jitter (~130 ps) were excluded from the analysis.

Although good agreement is seen between the streak camera and the FLI detector results, the similar curvatures of the two data sets, corresponding to two different oxygen concentrations, indicate systematic errors for both instruments (Fig. 4). The precision of the DIME detector, which is determined by the shot-to-shot fluctuation in the system, was measured. The standard deviation in fluorescence lifetime of a single pixel (σ_{total}), shown as error bars in Fig. 4, is approximately 120 ps. The precision is assumed to be limited mainly by image noise and camera gain fluctuations. Ten vertical pixels centered at H_0 in the FL images were analyzed, providing a standard deviation (σ_{noise}) of 100 ps, where systematic errors have been accounted for. Since the noise and camera gain fluctuations are independent, the standard deviation in fluorescence lifetime due to camera gain fluctuations (σ_{cgf}) was calculated to 70 ps. Hence, the relatively stable camera gain profiles of the ICCD cameras make image noise the limitation of the precision in the present experiments.
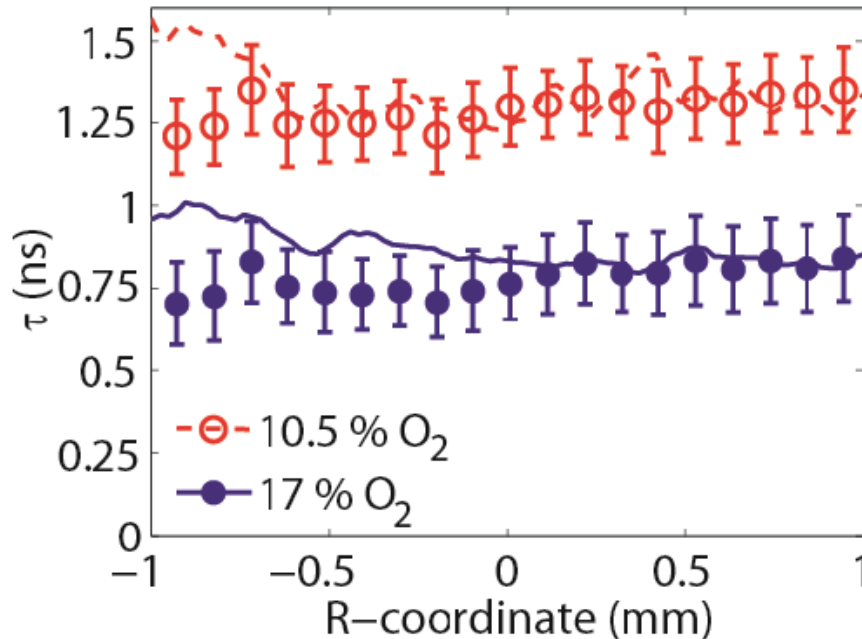

Fig. 4. Fluorescence lifetimes evaluated from 900 streak-camera accumulations (dashed and solid lines) as well as from single shot FLI detector images (filled and open circles with error bars). Two mixtures of oxygen and nitrogen were used as ambient quenching molecules; 10.5/89.5 (open circles and dashed line) and 17/83 (filled circles and solid line).

4. Sensitivity analysis

The experiment was modeled with Monte Carlo simulations to evaluate the signal-to-noise ratio propagation of the DIME algorithm. In order to present data that could be compared to previously reported simulated results [26], technical details regarding the specific detectors were not included. The noise propagation of an FLI method is commonly illustrated by calculating the figure of merit (F), which is formed as [27]:

$$F(\tau) = \frac{\sigma_\tau}{\tau} \cdot \left[\frac{\sigma_{N_{tot}}}{N_{tot}} \right]^{-1} \qquad (5)$$

Here, τ is the fluorescence lifetime, σ_τ is the standard deviation of the lifetime determination, N_{tot} the total number of photons detected by the two cameras, and σ_{Ntot}, the standard deviation of the number of detected photons. Similar to the signal detection simulation described above, the Monte Carlo calculations were performed for a pixel pair of the two cameras in a single excitation. For a span of fluorescence lifetimes, the arrival time of a photon at a certain detector is determined by three random samplings. These random samplings were

1. The number of photons collected from the volume that was imaged in a pixel. This number is randomly sampled from a Poisson distribution. The mean value of the number of collected photons can be varied to simulate different signal-to-noise ratios.

2. The probability of a photon to be directed to either of the two ICCD cameras at the beam splitter.

3. The arrival time of a photoelectron at the MCP. This probability density function is given by the normalized LIF-signal, seen as the red curve in Fig. 2.

After these three random samplings a number of photons end up at the two detectors at certain times. Using these arrival times as input data to the gain function (temporal gain profile) of the detector, the number of counts that each photon generates is determined. To calculate the signal strength, the number of counts generated by each photon, is summed for each camera. These data sets of simulated signals were analyzed using the DIME algorithm providing standard deviations and mean values of τ. The statistics of the total number of detected photons and fluorescence lifetimes were used to extract the figure of merit (Eq. (5)), which is plotted as a function of τ in Fig. 5. In these simulations, the beam splitter was set as 70/30, directing the majority of photons to the 2 ns camera. Furthermore, no difference in quantum efficiency and noise factors of the two cameras were included in the simulations, in order to provide results that could be compared to previously presented simulation data.

The experimental results from the two different oxygen concentrations are displayed with the same color coding as in Fig. 4. Roughly 100 LIF images from each camera were analyzed, accounting for inhomogeneous gain factors in different pixels. In these images, the detector noise (read-out noise, Johnson noise and dark-current noise) was found to be roughly 0.2% of the total noise.

The F-values for the experimental data were calculated by estimating the number of detected photons that were detected for each acquired image. To be able to present the experimental data with the simulated results, quantum efficiencies and noise factors of the two cameras were not taken into account. In a paper by McGinty et al. [28] a signal-to-noise characterization method was presented. The quadratic signal to noise in a pixel is expressed as

$$\left[\frac{I}{\sigma_I} \right]^2 = \frac{k^2 N_\gamma^2}{A N_\gamma^2 + k^2 E N_\gamma + \nabla_{CCD}^2} \qquad (6)$$
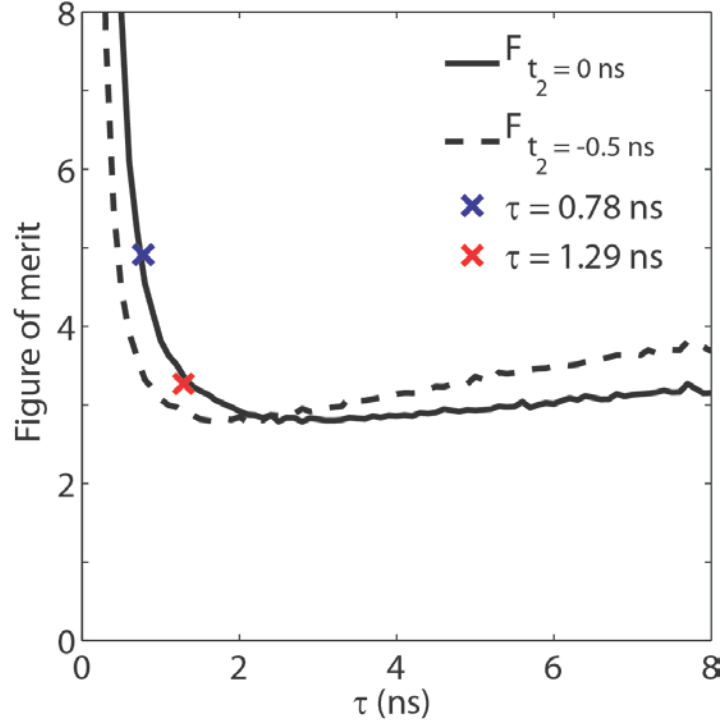
Fig. 5. The signal-to-noise propagation of the system is illustrated with the figure of merit (Eq. (5)). The experiment was modeled by Monte Carlo simulations for two different delay times for the 2 ns camera gain curve. The solid line corresponds to the settings that were used in the experiments, whereas the dashed line illustrates the figure of merit when the 2 ns camera gain function is advanced 0.5 ns in time. Evidently, the sensitivity of the technique is improved if the gain curve is temporally advanced but, on the other hand, less photons are detected, resulting in a degradation of the signal to nose ratio. The red and blue crosses are the experimental F-values corresponding to the measurement presented in Fig. 4 (the same color coding has been used).

where I/σ_I is the signal-to-noise ratio (SNR), k is the conversion factor from detected photons (N_γ) to signal counts (I). The detector noise is asserted ∇_{CCD}. McGinty et al. presented a recipe to determine the gain-dependent parameters A and E. In order to compare the experimental results to the simulations, A, E and ∇_{CCD} are assigned the values 0, 1 and 0 respectively. Even though the experimental data aligns well with the simulated results, the slight deviation is due to the fact that there is a relative difference in quantum efficiency and noise factor between the two cameras.

The sensitivity of the technique is changed if the delay time of the short gain function is shifted. To illustrate this change in sensitivity, two different figures of merit are displayed in Fig. 5 for different values of t_2. The solid line illustrates the figure of merit for the measurement settings used in the present experiments, whereas the dashed line represents the figure of merit with the short gain advanced 0.5 ns.

Instead of having a nonlinear relation between D and τ as in Fig. 3a, it would be advantageous to have a linear relationship between these parameters. A linear relationship would result with ramped gain functions. This choice was, however, not available on the cameras used in the current experimental setup. One of the gain profiles should increase over time and one should decrease:

$$G_1(t) = At \tag{7a}$$

$$G_2(t) = -At + AB \qquad (7b)$$

The ratio, $D(\tau)$, would then be given by

$$D(\tau) = \frac{I_0 A \int_0^\infty t e^{-t/\tau} dt}{I_0 A \int_0^\infty t e^{-t/\tau} dt + I_0 \int_0^\infty (-At + AB) e^{-t/\tau} dt} = \frac{\tau}{B} \qquad (8)$$

This kind of analysis is not limited only to LTI measurements. For instance, multiplication with ramped functions can be used on other timescales to determine lifetimes. This procedure could be beneficial in laser induced incandescence (LII) measurements as well as for
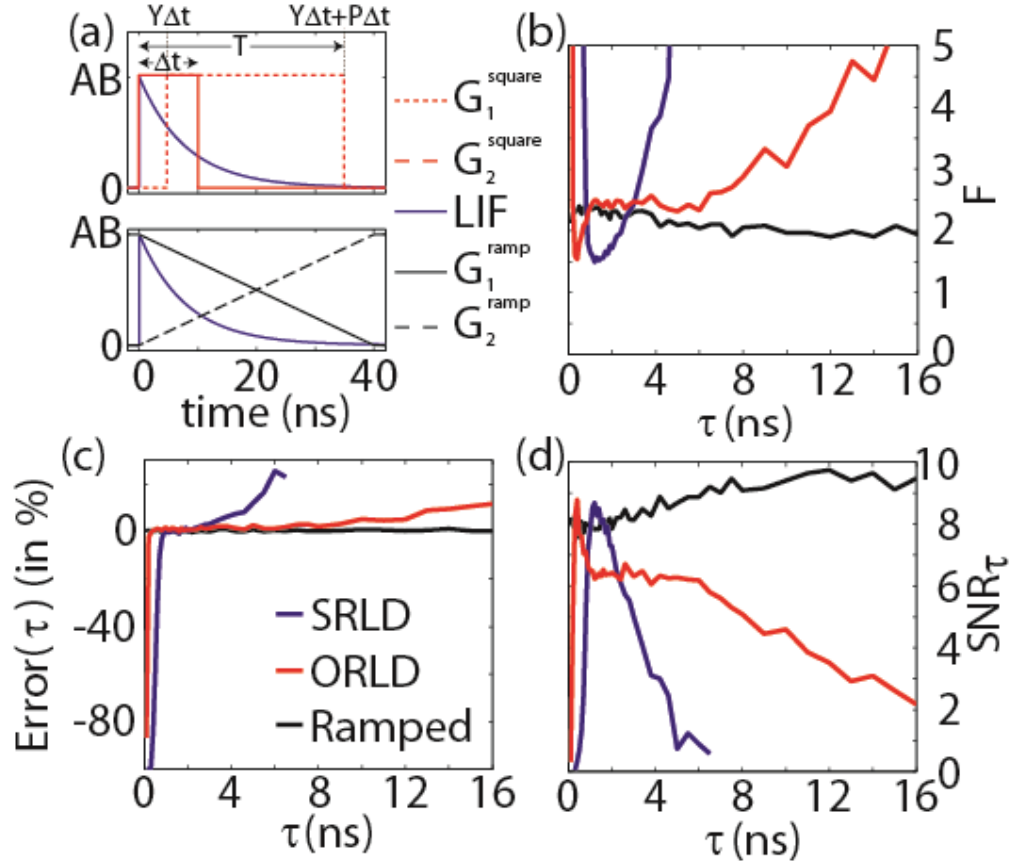

Fig. 6. Monte Carlo simulations of FLI with a mean value of 350 detected photons were performed for three different sets of gain functions. (a) The blue curve is a fluorescence curve with a lifetime of 8 ns. Detection using two square gain curves is seen in the upper plot. Two different approaches were tested; standard rapid lifetime determination (SRLD) and optimized rapid lifetime determination, proposed by Chan et al. [30]. For SRLD Δt is 3 ns, Y and P are 1 and T is 6 ns, meaning that we have two gain functions with equal width where the first one closes as the other opens. For ORLD Δt is 3 ns, Y is 0.25, P is 12 and T is 36 ns. In the lower plot, two ramped gain curves are used which are described by Eqs. (7a) and (7b) (the constant B is set to 40 ns). (b) The figure of merit corresponding to the simulated results using ramped gain curves is represented by the black curve. (c) The error of the mean value of the determined fluorescence lifetime. The SRLD as well as ORLD are unable to predict short lifetimes since the signal enhanced by the latter of the two gain functions (dashed red curve) is very weak. For longer lifetimes, the SRLD breaks down. (d) The SNR for the detected fluorescence lifetime is nearly constant for the ramped-gain curve configuration. The square gain configurations have lifetime dependences on their SNR with clear optima.

phosphorescence studies. It should also be pointed out that a linear relationship between D and τ could be obtained by using one ramped and one flat gain profile. The ratio should simply be formed by dividing the two signals with each other having the signal acquired with a constant gain curve in the denominator. From an engineering point of view that might be the simplest way of implement RGP-LD in FLI. Monte Carlo simulations with a mean value of 350 events (in total) per measurement were performed with ramped and square gain profiles, as shown in Fig. 6a. In Fig. 6b, F is plotted for the two sets of gain profiles. While the sets of square profiles result in low figure of merits at certain lifetimes, the ramped set of gain profiles gives a nearly constant figure of merit around 2.

Not only does the scheme provide an F-value that is virtually insensitive to the lifetime, but it also results in less error at lower SNR, as can be seen in Fig. 6c, especially for shorter lifetimes. Furthermore, with both gain profiles being non-zero throughout the entire signal, the absolute maximum number of events (photons or electrons) is acquired. Therefore, using the RGP-LD algorithm in combination with DIME would be ideal since it gives a very high SNR, which is crucial in single shot detection of weak signals. In addition, the DIME algorithm would account for imperfections in the ramped gain profiles. The advantage of high collection efficiency is clearly seen in the SNR at different lifetimes shown in Fig. 6d. For the RGP-LD, the SNR merely depends on signal strength while the sets of square gain functions suffer from low SNR at short and long fluorescence lifetimes due to inefficient detection.

5. Discussion

We have developed and demonstrated a new detector approach for single-laser shot 2D fluorescence lifetime imaging. The technique offers the possibility to determine lifetimes of rapid dynamic events with acquisition times of the same order of magnitude as the fluorescence lifetimes, which in this experimental investigation span from 0.8 to 7 ns. This span of lifetimes is more than an order of magnitude lower than what was presented by Ni and Melton [9]. Furthermore, single-laser shot results with a standard deviation of roughly 120 ps show excellent agreement with accumulated streak camera data. Hence, the current study proves that the DIME detector approach, due to its superior sensitivity as well as 2D visualization capacity, is a far better tool than the streak camera for measurements of effective lifetime.

It ought to be mentioned that while the acquisition time for a single fluorescence lifetime image is determined by the signal decay time and, hence, is at a minimum, the current repetition rate of 10 Hz is the limitation when producing movies of dynamic events. For the current setup, the repetition rate is limited by the repetition rate of the laser. However, the DIME concept is by no means restrained to the current setup, and the upper limit of the frame rate is determined by the signal decay time since the signal needs to decay to zero before a new excitation is performed. If single-shot measurements are not of interest, it is enough to include a single camera in the setup and use different gain characteristics when acquiring the two images. However, also single-shot acquisitions can be obtained using a single camera. Agronskaia et al. [29] demonstrated a scheme in which the fluorescence signal was split into two parts and one part was delayed through an optical delay line. The two signal parts were then imaged onto different halves of the camera chip. The final part of the fluorescence decay was detected by the initial part of their camera gain and the initial part of the fluorescence decay was detected after the delay line by the final part of the camera gain. Not only would such a scheme allow single-shot measurements, but it would also benefit from DIME since the initial and final parts of a gain curve always deviate from perfectly vertical flanks. In addition, since the rise and fall of gain curves often are ramp-like, the relation between D and τ could potentially be close to linear. Nevertheless, using an optical delay line will decrease the signal intensity since the fluorescence signal is not collimated. Another way to obtain single-shot lifetime images would be to use a multi-channel segmented gated optical intensifier, such as the one used by Elson et al. [19] for sequential time gated FLI. By using

DIME, the signal-to-noise ratio could be improved significantly as compared to using sequential time gating.

Monte Carlo simulations of the experimental detection show good agreement with experimental data (Fig. 5). Furthermore, simulation performed with the short gain profile advanced in time showed higher sensitivity for shorter fluorescence lifetimes. When the camera gain is closing earlier, merely the closing flank of the gain function is used. On one hand, this choice offers higher sensitivity for shorter lifetimes, but on the other hand fewer photons are detected, resulting in lower SNR. In general, LIF-imaging of rapid events allows only a few or no accumulations and it thus has an inherent problem with low SNR. However, a gain profile advanced in time can be compensated for by using a beam splitter with higher splitting ratio to raise the SNR for the camera with the short gain function.

The DIME concept uses the actual shapes of the camera-gain profiles instead of idealized square gain profiles that have been used in prior attempts to perform FLI in single-shot measurements. Using gain profiles that very closely resemble top-hat shapes is more difficult to apply to single-shot measurements than non-top hat profiles since several gain profiles must fit under the signal decay, thus requiring extremely short gain functions. Top-hat profiles also mean that fewer photons are collected under each gain function than what is possible with non-top hat profiles in combination with DIME. One of the strengths using DIME is that gain profiles wider than the signal decay can be used, allowing as many photons as possible to be collected under each gain profile. It should be mentioned that there could potentially be different gain characteristics in different camera pixels, making the extraction of the gain functions more tedious. Analysis of the 2 ns gain used in the current study revealed an irising effect. However, this effect is most pronounced at the edges of the image and since the region of interest was located on the central part of the CCD chip, the irising effect could be neglected. In addition, since each pixel is analyzed separately, it is possible to add a delay of the gain curve as a function of pixel position if necessary. Still, with adequate signal-to-noise ratio nothing prevents the measurement of the gain curve of each pixel.

The FLI scheme that most closely compares to DIME would be dual gain curve detection analyzed by the standard rapid lifetime determination (SRLD) routine, as proposed by Ashworth and associates [18] and the further developed optimized rapid lifetime determination algorithm (ORLD) presented by Chan et al. [30]. All three experimental approaches are applicable in wide-field imaging that could be used for single-shot measurements with data analysis in the temporal domain. Even though SRLD offers an elegant analytic expression for lifetime determination, it does not reflect the intensifying process of an ICCD camera for shorter fluorescence lifetimes since ultra-short gain functions are quite far from top-hat profiles. This systematic error is also incorporated in the ORLD algorithm which, on the other hand, has a solution that needs to be found numerically. Since this error depends on the actual shape of the particular camera gain function used in an experiment, a direct comparison is not straight forward. If single-shot measurements are to be undertaken, two gain curves have to be used. These gain functions will almost certainly possess different gain profiles, which would introduce even larger errors. More interesting, however, is that modulated gain functions can be used to provide higher signal to noise ratio as well as higher sensitivity when lifetimes are determined with the DIME algorithm. Hence, a possibility to design the shape of the gain functions would allow for optimization of DIME for the span of fluorescence lifetimes of interest for a particular study. The cameras used in these experiments were not equipped with such a feature. The result showed that ramped gain profiles would provide equally high sensitivity for any lifetime. However, a controlled detector scheme, such as DIME, should be used if possible to calculate the relationship between image ratios and the fluorescence lifetime instead of using analytic expressions. These analytic expressions serve as guidelines for optimal choices of gain functions and should only be considered as approximations.

In comparisons with prior single-shot lifetime approaches using Ashworth's SRLD algorithm [18] and ORLD, proposed by Chan et al. [30], we present a detection scheme with higher accuracy, sensitivity and collection efficiency for rapid lifetime imaging applications than earlier proposed schemes. When comparing the present results to frequency domain FLI, it should be stressed that the accumulation time is significantly longer for frequency domain measurements. Therefore single-shot measurements in the frequency domain can simply not be performed on the same time scale. However, Edler et al. [26] showed analytical expressions along with Monte Carlo simulations for several FLI schemes in the frequency domain. For lifetimes between 0.5 and 1.5 ns, the minima of calculated F-values for sinusoidal gain modulations and excitations were in the range 6-9, whereas Dirac excitation in combination with sinusoidal gain modulation resulted in minimum F-values as low as 2. Nevertheless, the F-values of these schemes depend strongly on the lifetime of the signal, hence requiring *a priori* information regarding the fluorescence lifetime. For the gain functions used in experiments presented in the current study, the F-value was roughly 4 for a lifetime around 1 ns (Fig. 5). The minimum F-value (~2.7) was obtained for lifetimes around 3 ns. Figure 5 also shows that the F-value can be improved for short fluorescence lifetimes by advancing the short gain function in time. F-values obtained with the gain functions used in presented experimental data depend on the lifetime of the signal, just as for frequency domain FLI. In order to obtain F-values which are virtually independent of the lifetime, DIME could be used in combination with ramped gain profiles (Fig. 6). Using such a scheme would also yield F-values around 2.5, which is comparable to the lowest values obtained in the simulations by Edler et al. [26].

We believe that this new approach, combining dual imaging modeling evaluation (DIME) with ramped gain profiles-lifetime determination (RGP-LD), will be a valuable tool for future investigations of fluorescence lifetimes in a wide variety of research fields.

Acknowledgments